Magnetic resonance in spherical Co-Ni and Fe-Co-Ni particles

D. Mercier and J.-C. S. Lévy*
Laboratoire de Physique Théorique de la Matière Condensée, Case 7020, Université Paris 7, 2 Place Jussieu, 75251 Paris Cedex 05, France

G. Viau, F. Fiévet-Vincent, and F. Fiévet
Laboratoire de Chimie des Matériaux Divisés et Catalyse, Case 7090, Université Paris 7, 2 Place Jussieu, 75251 Paris Cedex 05, France

P. Toneguzzo and O. Acher
Commissariat à L'Energie Atomique, Le Ripault, BP 16, 37260 Monts, France
(Received 7 December 1999)

Magnetic resonance is studied in absence of external field on composite materials made up with spherical and monodisperse fine Co–Ni and Fe–Co–Ni particles. The particle size range varies over one order of magnitude from 25 to 250 nm. In the frequency range studied [0.1–18 GHz] several resonance bands are generally observed attributed to nonuniform resonance modes. The resonance frequencies are found to depend on the magnetic particle size, only weakly for the lowest frequency mode, in a more pronounced manner for the following modes. A theoretical model based on a discrete treatment of the resonant effect in independent small spherical or cylindrical grains is proposed. It allows to compute the resonance frequencies, the spin-wave profiles, and the spin-wave intensities. The respective influences of particle geometry, surface pinning, crystalline anisotropy, and exchange parameter values are presented. According to this model it is found that the size dependence of the resonance frequencies is mainly related to the surface pinning and to the exchange parameter value. In all cases the size dependence of the lowest frequency mode is found weaker than that of the following modes and for large particles the frequency of the first mode is directly related to the crystalline anisotropy. The particle shape effect on resonance frequencies is weak whereas the spin-wave profiles of the first modes are found to depend on the particle geometry. This model enables us to describe the general shape of the experimental spectra and to infer the magnetocrystalline anisotropy constants (K_1) from the experimental data, which are found in good agreement with bulk values. Moreover it shows that the weak size dependence of the lowest frequency mode is due to a weak pinning at the particle surface. Nevertheless, the effect of particle size on higher spin-wave modes requires us to account for the magnetic interactions between grains.

I. INTRODUCTION

Recently the interest in metallic particles also called metallic grains has been strongly increased since efficient routes to make grains with well-defined characteristics appeared. This is the case of physical ways and of chemical ways as well. First, small and large clusters have been produced in atomic beams under ultrahigh vacuum with an accurate size selection for more than ten years.[1] Then, the preparation of layered materials *ABAB*... by means of molecular-beam epitaxy is known to lead sometimes to self-organization processes with the production of nearly spherical inclusions of material *A* in a matrix *B*, specially when materials *A* and *B* are immiscible in the bulk. This can be the case for a metallic material *A* and a metallic material *B*,[2] or for a metallic material *A* and an insulating oxide *B*[3] with the result of magnetic grains inserted in a matrix. Well-defined metallic grains can also be obtained through chemical routes: by decomposition of organometallic precursors,[4] reduction from homogeneous solutions,[5] or in microemulsions.[6,7] In these liquid phase processes the control of the particle morphology is achieved by a careful control of the nucleation and growth steps of the solid particles. Since many metallic materials are magnetic, the preparation of magnetic metallic grains opens the very rich and active field of magnetic grains with numerous physical effects such as superparamagnetism,[8] giant magnetoresistance,[9] or mesoscopic transport effects in magnetic tunnel junctions[10] for instance. These materials display physical properties related to surface or quantum size effects.

In the present paper we are interested in spherical alloyed particles of magnetic elements such as cobalt, nickel, and iron, which are prepared by a chemical way. The observed physical property here is magnetic resonance, which is well known to be very sensitive to the sample size, at least in the case of thin films.[11] Thus, by analogy, magnetic grain resonance is expected to be sensitive to grain size and grain composition. The preparation of monodisperse particles over a wide range of size and composition, allows an accurate comparison between experimental results and models. Recently several of Aharoni's works[12,13] dealt with exchange modes both in spherical and in cylindrical grains of radii *R* within a continuum approach. With the same approach the eigenvectors were also computed.[14] A R^{-2} law for the behavior of eigen frequencies is found.[12] The comparison of this last conclusion with experimental results on very small spheres of Fe–Co–Ni or Co–Ni alloys[15] shows that such a

R^{-2} law is not observed for the resonance frequencies. We present here results upon magnetic resonance in small spherical particles. The size range presented has been extended toward nanometer size particles and covers one order of magnitude: 25–250 nm. Attention has been paid to the size dependence of the different modes observed. Moreover, in order to have a better understanding of the experimental results a discrete treatment of the resonant effect in independent small spherical or cylindrical grains is proposed.

The sample preparation is indicated in Sec. II while the experimental investigation of dynamic properties is reported in Sec. III. Section IV deals with the model and comparison with the experimental results. Finally conclusions are deduced.

II. EXPERIMENT

A. Preparation of monodisperse ferromagnetic metal powders

Ferromagnetic $Co_xNi_{(100-x)}$ and $Fe_z[Co_xNi_{(100-x)}]_{(1-z)}$ particles were prepared by precipitation in 1,2-propanediol according to a procedure reported in detail previously.[16,17] Nickel, cobalt, and iron are produced in this medium by reduction upon heating of nickel(II) and cobalt(II) hydroxides and by disproportionation of iron(II) hydroxide, respectively. Reaction of mixed hydroxides yields polymetallic particles. $Co_xNi_{(100-x)}$ particles with x varying in the whole composition range can be synthesized by this method since both Co^{II} and Ni^{II} are quantitatively reduced by the polyol. For $Fe_z[Co_xNi_{(100-x)}]_{(1-z)}$ particles the composition range available is limited to $0<z<0.25$ by the disproportionation of Fe(II), while x varies in the range 0–100.

Metallic particles are formed by nucleation and growth from the solution. Upon controlled experimental conditions the mixed hydroxide plays the role of a reservoir phase, the dissolution of which releases slowly M(II) species in the solution. In this way the growth step of the particles can be controlled.[16] Hence a complete separation between nucleation and growth steps can be achieved and thus monodisperse particles are obtained. Spontaneous nucleation leads to CoNi particles in the micrometer size range (typical mean diameter $d_m=2\ \mu$m)[16] and to FeCoNi particles in the submicrometer size range ($d_m=0.2\ \mu$m typically).[17] An accurate control of the particle mean size can be obtained through heterogeneous nucleation: a small amount of a precious metal salt is readily reduced *in situ* by the polyol to give ultrafine metal particles that act as heterogeneous nuclei for the further growth of $Co_xNi_{(100-x)}$ and $Fe_z[Co_xNi_{(100-x)}]_{(1-z)}$ particles. By varying the molar ratio of precious metal upon ferromagnetic metal it is possible to control the average diameter of the final ferromagnetic particles. $AgNO_3$ and K_2PtCl_4 appeared as complementary nucleating agents for heterogeneous nucleation in liquid polyols. By varying the molar ratio [M]/[Co+Ni+Fe] (M=Ag or Pt) in the range 10^{-6}–10^{-4} ferromagnetic particles were obtained with average diameter in the ranges 200–500 nm and 20–150 nm using silver nitrate and platinum tetrachloride, respectively.[18] In this last case, the size of the platinum nuclei was estimated to 2–3 nm.[18]

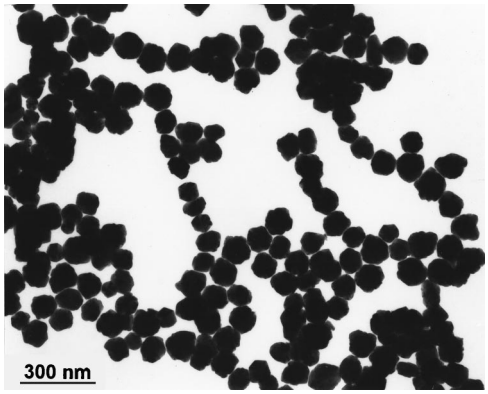

FIG. 1. TEM image of $Co_{65}Ni_{35}$ particles ($d_m=93$ nm; $\sigma=11$ nm) prepared in propanediol by heterogeneous nucleation with Pt/(Co+Ni)=2.5×10^{-5}.

B. Powders characterization

The particles have, generally, an almost spherical shape, a narrow size distribution (the standard deviation of the size distribution inferred from image analysis of ~250 particles is found to be less than 15% of the mean diameter) and a limited agglomeration as exemplified in Fig. 1. Nevertheless, the finest CoNi samples are not made up of spherical particles but of faceted isotropic particles.

$Co_xNi_{(100-x)}$ and $Fe_{0.13}[Co_xNi_{(100-x)}]_{0.87}$ powders appeared always as crystalline by x-ray diffraction with a pattern varying with the composition. High-nickel content powders ($x<35$) crystallize as a single fcc phase. High-cobalt content powders ($x>35$) crystallize as a mixture of two close-packed phases with a fcc and a hcp lattice, respectively. The fcc lattice parameter was found to vary linearly versus x all over the composition range from the nickel parameter ($a=0.352\,38$ nm) to the cobalt one ($a=0.354\,47$ nm). This verification of Vegard's law allows us to describe this phase as an alloy of the two metals.[19] The x-ray diffraction line broadening analysis following the Williamson and Hall method[20] showed that for the CoNi particles the main contribution to the broadening comes from stacking faults, mainly in the hcp phase. For the FeCoNi particles, an additional contribution comes from the small crystallite size. Transmission electron microscopy (TEM) observations and selected area electron diffraction on isolated particles confirmed that the CoNi particles are made up by a few number of crystallites whereas the iron-based polycrystalline particles are made up of a large number of small crystallites. Structural and textural characteristics of the powders do not present any significant change when the mean size of the particles varies.

Chemical analysis showed that carbon and oxygen are the main impurities. They were found in low contents in large particles (e.g., 0.5 wt. % and 1.4 wt. % for C and O respectively, in $Co_{80}Ni_{20}$ particles with $d_m=220$ nm). Powder density ρ and saturation magnetization at room temperature M_s are close to bulk values for the large particles (8.5 g cm^{-3} and 135 emu g^{-1}, respectively for $Co_{80}Ni_{20}$ particles with $d_m=220$ nm). When the particle size decreases C and O contents increase whereas ρ and M_s decreases; in all cases the variations with the size follows a d_m^{-1} dependence. These physicochemical characterizations allow us to describe the

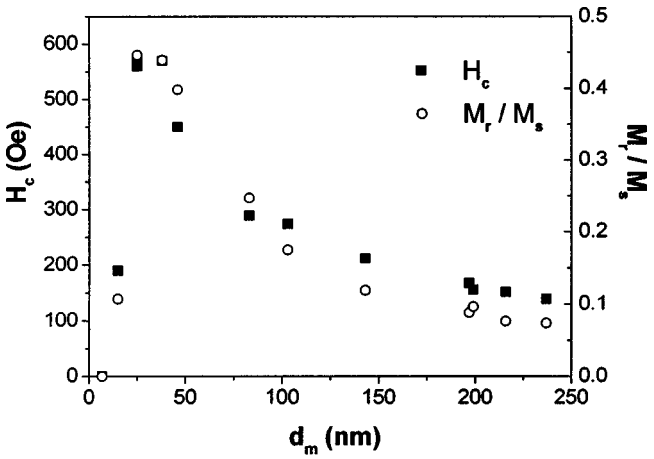

FIG. 2. Coercivity H_c and remanence to saturation magnetization ratio M_r/M_s at room temperature of $Co_{80}Ni_{20}$ particles vs mean diameter.

particles as made up with a metallic and ferromagnetic core surrounded by a thin nonmetallic layer.[19] Saturation magnetization and density of the metallic core were found very close to the bulk values. The thickness of the nonmetallic layer was estimated in the range 2–3 nm and independent of the particle size.

Static magnetic measurements at room temperature were performed on compacted powders with an hysteresismeter SIIS 2000. The powder coercivity H_c and remanent to saturation magnetization ratio M_r/M_s were found to depend on the particle size. For a given composition, when the particle size decreases, H_c and M_r/M_s increase steadily to reach a maximum and then decrease sharply to zero (Fig. 2). The critical size corresponding to the maximum of coercivity and remanence lies between 20 and 40 nm according to the chemical composition.[21] For that size the M_r/M_s ratio reaches the values of 0.45 and H_c, several hundreds of Oe (higher is the Co content, higher is the value of the maximum of coercivity). So, when the particle size decreases from 250 to about 25 nm the magnetic configuration goes from a polydomain to a monodomain configuration, which is

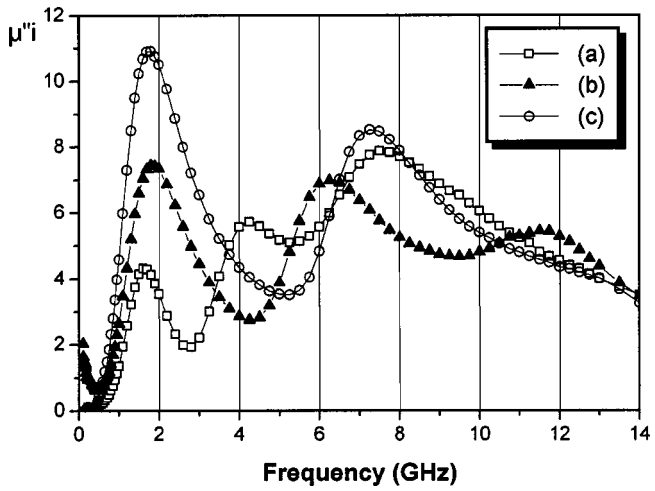

FIG. 4. Imaginary part of the intrinsic permeability vs frequency of $Co_{80}Ni_{20}$ particles (a) $d_m = 142$ nm, (b) $d_m = 82$ nm, and (c) $d_m = 62$ nm.

responsible for the increase of H_c and M_r/M_s values. Below 25 nm, the effect of thermal fluctuations has consequences to decrease H_c and M_r/M_s values, and below 7 nm a superparamagnetic behavior is observed at room temperature. Thus, within the investigated range [25–250 nm] for dynamic magnetic properties, the smallest particles tend to a monodomain configuration but do not present a superparamagnetic behavior at room temperature.

III. DYNAMIC MAGNETIC PROPERTIES

The microwave characterizations were carried out on nonconducting composite materials having high-volume concentrations of magnetic inclusions. Such composites were made by compacting the metal powders previously coated by a manganese oxide thin layer through a chemical treatment in acidified aqueous solutions of potassium permanganate.[21] The coating of the particles appears by TEM to be quite homogeneous with an average thickness of about 10 nm. The ferromagnetic particle volume concentration in the com-

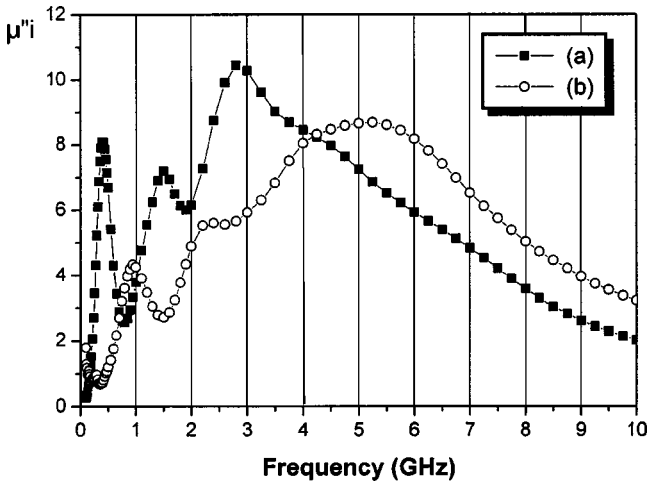

FIG. 3. Imaginary part of the intrinsic permeability vs frequency of (a) $Fe_{0.13}[Co_{50}Ni_{50}]_{0.87}$ particles, $d_m = 206$ nm, (b) $Co_{50}Ni_{50}$ particles, $d_m = 250$ nm.

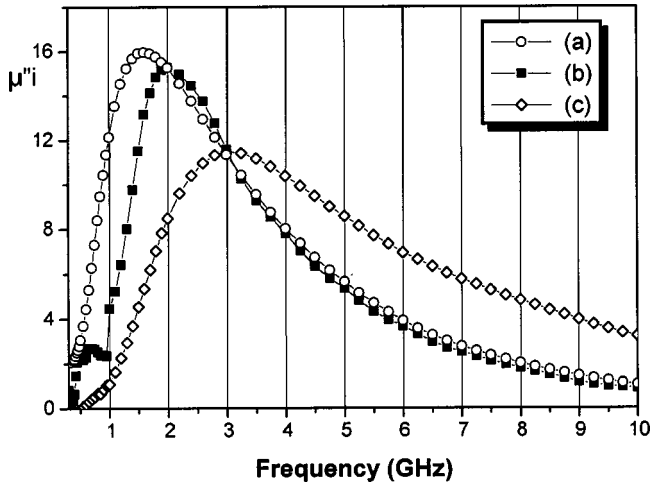

FIG. 5. Shift of the resonance frequency with Co content for $Co_xNi_{(100-x)}$ nanoparticles: (a) $Co_{35}Ni_{65}$ $d_m = 50$ nm, (b) $Co_{50}Ni_{50}$ $d_m = 50$ nm, and (c) $Co_{80}Ni_{20}$ $d_m = 34$ nm.

pacted samples was determined with accuracy, from the mass and the volume of the sample, the saturation magnetization of the coated powder, and from the saturation magnetization and density of the as-made powder. This concentration varies between ~25% for the finest particles and 50% for the largest ones.

The microwave properties $[\varepsilon(\omega), \mu(\omega)]$ were measured in the 0.1–18 GHz range with a APC7 coaxial line associated with a network analyzer HP8510. Measurements were conducted in the absence of an external magnetic field. The permitivity $\varepsilon(\omega)$ of these composite materials was found low and constant on the whole frequency range studied. No dielectric losses were observed $[\varepsilon''(\omega)=0]$.

The microwave properties of composite materials are very dependent on the magnetic particle concentration. The comparison of the properties of different particle concentration materials is made easier through the comparison of the intrinsic permeability of the particles calculated according to the formula[22]

$$\mu_i=\frac{\mu_e[2\mu_e+\mu_m(3q-2)]}{\mu_e(3q-1)+\mu_m},$$

with μ_i the particle intrinsic permeability, μ_e the material permeability, μ_m the matrix permeability ($\mu_m=1$ in our case), and q the volume concentration of the particles in the material.

Previous studies clearly showed that the dynamic permeability in the microwave range of micrometer sized particles presents a single and very broad band.[23] For particles with a mean diameter lower than about 400 nm several bands appear in the frequency range investigated, for CoNi and FeCoNi particles as well (Fig. 3).

The accurate control of the particle size allowed by the synthesis process affords the possibility to follow the size dependence of the different resonance bands for several chemical compositions. For the largest particles, several resonance bands close to each others are observed (Fig. 3). Both the resonance band frequencies and their relative intensities are found to vary with the particle mean size. As exemplified in Fig. 4 for $Co_{80}Ni_{20}$ particles, when the particle size decreases, an overall shift of the bands toward high frequencies is observed and the relative intensity of the lowest frequency resonance band increases steadily. For the smallest particles, the bands become less and less close to each other, the number of bands observed in the range studied 0.1–18 GHz decreases, and the relative intensities of the highest frequency resonance bands decrease. Below a mean diameter, which is about 50 nm for every composition studied, a single band only remains in that range (Fig. 5).

Despite an overall shift when d_m decreases, it is noteworthy that all the resonance frequencies do not present the same size dependence. As shown in Figs. 6(a)–6(c) the first band frequency increases very slowly when the particle size decreases within a large range. It is only for the smallest particles that a significant shift is observed. At the opposite a far more important shift is observed for the following bands as the mean size decreases in the submicrometer range.

The influence of chemical composition on the resonance bands frequency has been studied. For both $Co_xNi_{(100-x)}$ and $Fe_z[Co_xNi_{(100-x)}]_{(1-z)}$ systems, at a given particle size, the resonance bands of the permeability curves are shifted toward high frequencies when the Co content increases from $x=20$ to 100. This is exemplified on the permeability curves of nanometer sized particles (Fig. 5) and by the comparison of the resonance frequencies of submicrometer sized $Co_xNi_{(100-x)}$ particles in Figs. 6(a)–6(c) [see also Ref. 23(a)]. Moreover low-iron content in the ferromagnetic particles composition has a significant influence on their perme-

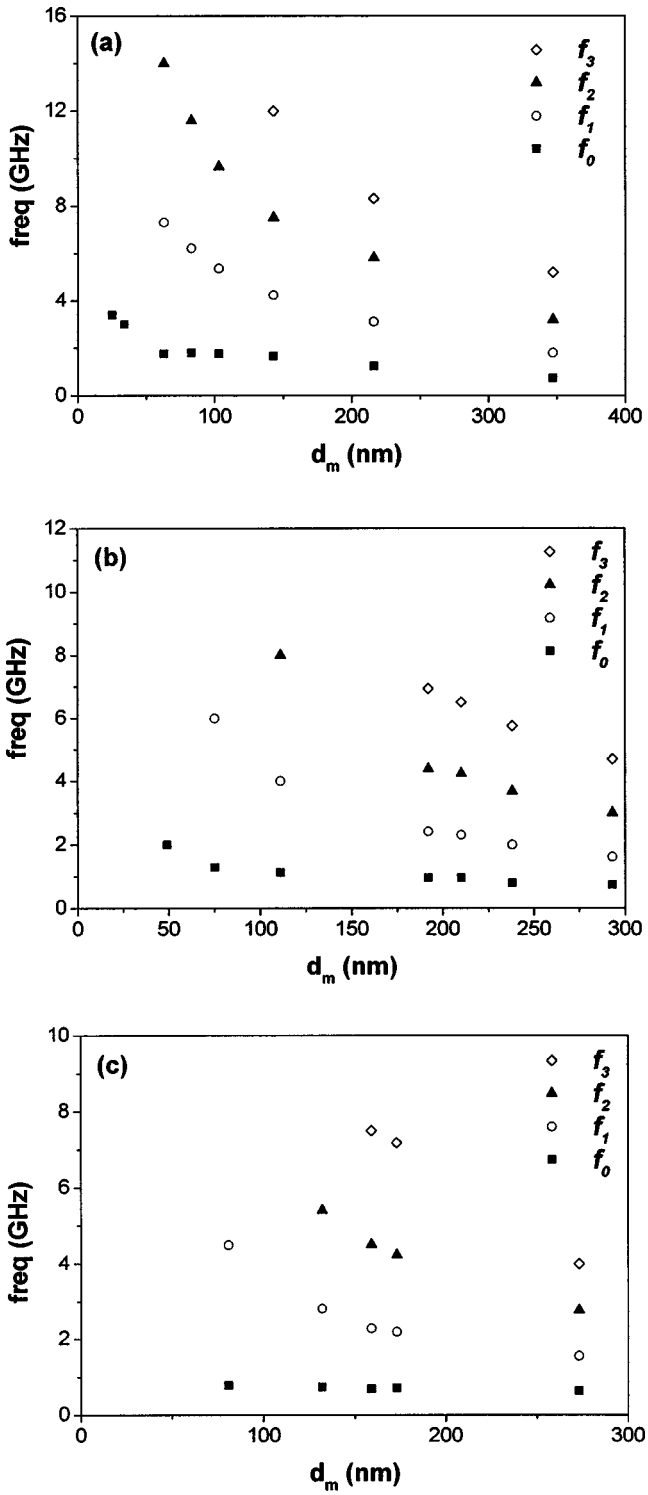

FIG. 6. Resonance frequencies of microwave permeability vs mean radius of (a) $Co_{80}Ni_{20}$ particles, (b) $Co_{50}Ni_{50}$ particles, and (c) $Co_{20}Ni_{80}$ particles.

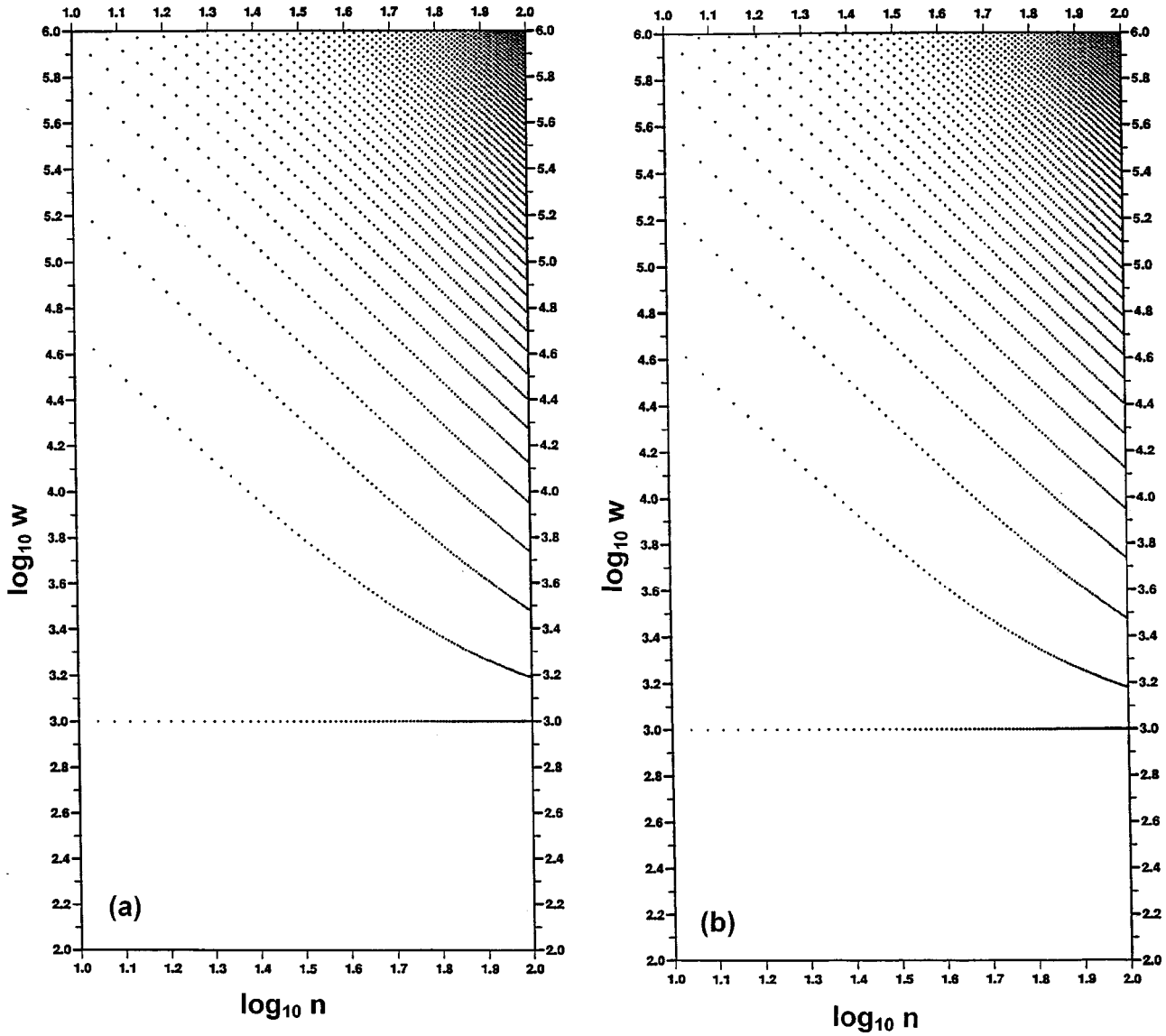

FIG. 7. The resonant frequency as a function of the radius in a $\log_{10}-\log_{10}$ plot with $J=10^6$ G and $h=1000$ G for (a) a spherical grain with an unpinned outer surface, (b) a cylindrical grain with an unpinned outer surface, and (c) a spherical grain with a pinned outer surface.

ability. From the comparison of the permeability of $Fe_{0.13}[Co_xNi_{(100-x)}]_{0.87}$ and $Co_xNi_{(100-x)}$ particles with a similar mean diameter and a same Co/Ni ratio, it is shown that the resonance bands appear at lower frequencies for the iron-based particles than for iron-free particles (Fig. 3).

IV. MODEL OF SPIN-WAVE RESONANCE IN SPHERICAL AND CYLINDRICAL GRAINS

The discrete treatment of the resonant effect we developed here is based upon the idea that realistic finite-size effects are essential in the determination of spin waves in grains. It deals with independent small spherical or cylindrical grains. First, either from a quantum treatment of the equation-of-motion for a spin Hamiltonian with exchange interaction, magnetic anisotropy, and Zeeman effect, or from a classical treatment of the Landau-Lifshitz equations with Gilbert damping, the equation of evolution for local magnetization is easily deduced within a continuum model.[12]

$$\frac{\partial \mathbf{M}_i}{\partial t}=\gamma[\mathbf{M}_i\wedge(\mathbf{H}_0+\mathbf{H}_{A_i}+\mathbf{H}_{\mathrm{ex}})+\lambda\mathbf{M}_i\wedge\langle\mathbf{M}\rangle_i], \qquad (1)$$

where the exchange field $\mathbf{H}_0$ is deduced from the magnetization Laplacian by $\mathbf{H}_0=Da_0^2\Delta\mathbf{M}=J\Delta\mathbf{M}$, with the exchange constants D and J and the lattice parameter a_0, the local anisotropy field is $\mathbf{H}_A$ and λ is the Gilbert damping parameter, which is taken as null here. The local anisotropy field results from the sum of a uniform crystalline anisotropy field $\mathbf{H}_A$, of the demagnetizing field, and of the external field $\mathbf{H}_{\mathrm{ex}}$. The details of the magnetostatic interaction between spins, leading to terms other than the demagnetizing field, are here neglected in a simple approach. Assuming a resonant process with an oscillating part of the magnetization $\mathbf{M}(t):\mathbf{m}(t)\sim\exp(-i\omega t)$, the equation-of-motion reads:

$$-i\omega\mathbf{m}=\gamma\mathbf{M}\wedge(J\Delta\mathbf{M}+\mathbf{H}_A+\mathbf{H}_{\mathrm{ex}}). \qquad (2)$$

With a coordinate system where the z axis is collinear with the effective magnetic field and thus with the static part

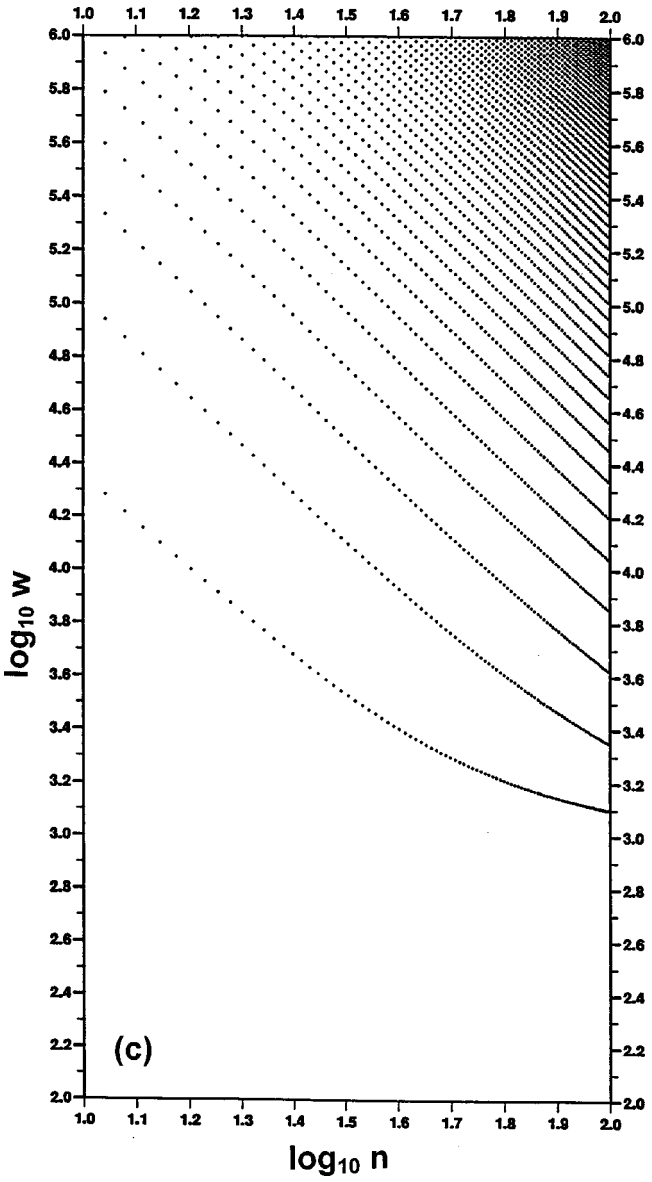

FIG. 7. (*Continued*).

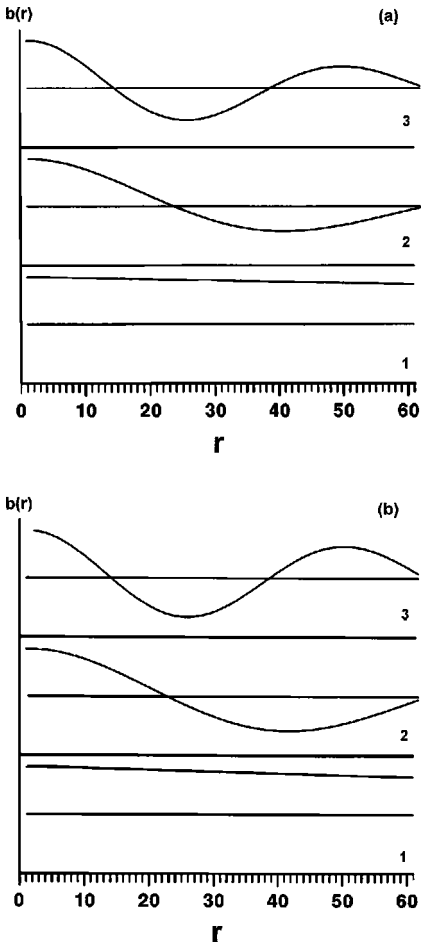

FIG. 8. The spin-wave profiles $b_i(r)$ of the first three modes of a grain with a pinned outer surface, with $J=10^6$ G for (a) a spherical grain and (b) a cylindrical grain.

M_z of magnetization, ΔM_z can be neglected. Here both the anisotropy field and the external field are assumed to be collinear with the z axis, so the equations-of-motion for the magnetization components read

$$-i\omega m_x=\gamma[m_y(H_{Az}+H_{exz})-M_zJ\Delta m_y],$$

$$-i\omega m_y=\gamma[-m_x(H_{Az}+H_{exz})+M_zJ\Delta m_x]. \qquad (3)$$

With this approach, for every grain a uniform orientation of the effective magnetic field is assumed within each grain. At the grain level it means that each grain contains only a few magnetic domains and that their common crystalline orientation defines the crystalline anisotropy easy axis. Thus no external field is required to magnetically orient the sample, and in such a case, which is close to the experimental one, the effective field is just the anisotropy field with the addition of the demagnetizing field due to magnetized parts. For the whole grain set, this approach means that all grains share a common crystalline and magnetic orientation. As a matter of fact such a common orientation between grains is obviously imposed by dipolar interactions that define the demagnetizing field in the sample. This common orientation has been observed in numerous numerical computations of the magnetic and structural nematiclike order of grain chains when magnetic spheres interact via magnetic dipolar interactions and short-ranged repulsive interactions.[24,25] Thus this common ''nematic'' anisotropy axis is well justified here from dipolar considerations even in the present experimental situation of magnetic resonance without external field.

Introducing the complex variable $m=m_x+im_y$, the equation-of-motion of this complex magnetization reads

$$\Delta m+\frac{1}{JM_z}\left(\frac{\omega}{\gamma}-H_{Az}-H_{exz}\right)m=0, \qquad (4)$$

which looks like a Schrödinger equation on m and was solved by means of Bessel functions by Aharoni.[12] With a cylindrical geometry as valid for granular rods, it reads more explicitly

$$\left[\frac{\partial^2}{\partial r^2}+\frac{1}{r}\frac{\partial}{\partial r}+\frac{1}{r^2}\frac{\partial^2}{\partial\theta^2}+\frac{1}{JM_z}\left(\frac{\omega}{\gamma}-h\right)\right]m=0, \qquad (4a)$$

where h is the uniform effective field in the z direction, as discussed before. In this geometry, because of periodicity in the cylindrical angle θ, the eigenmodes are characterized by

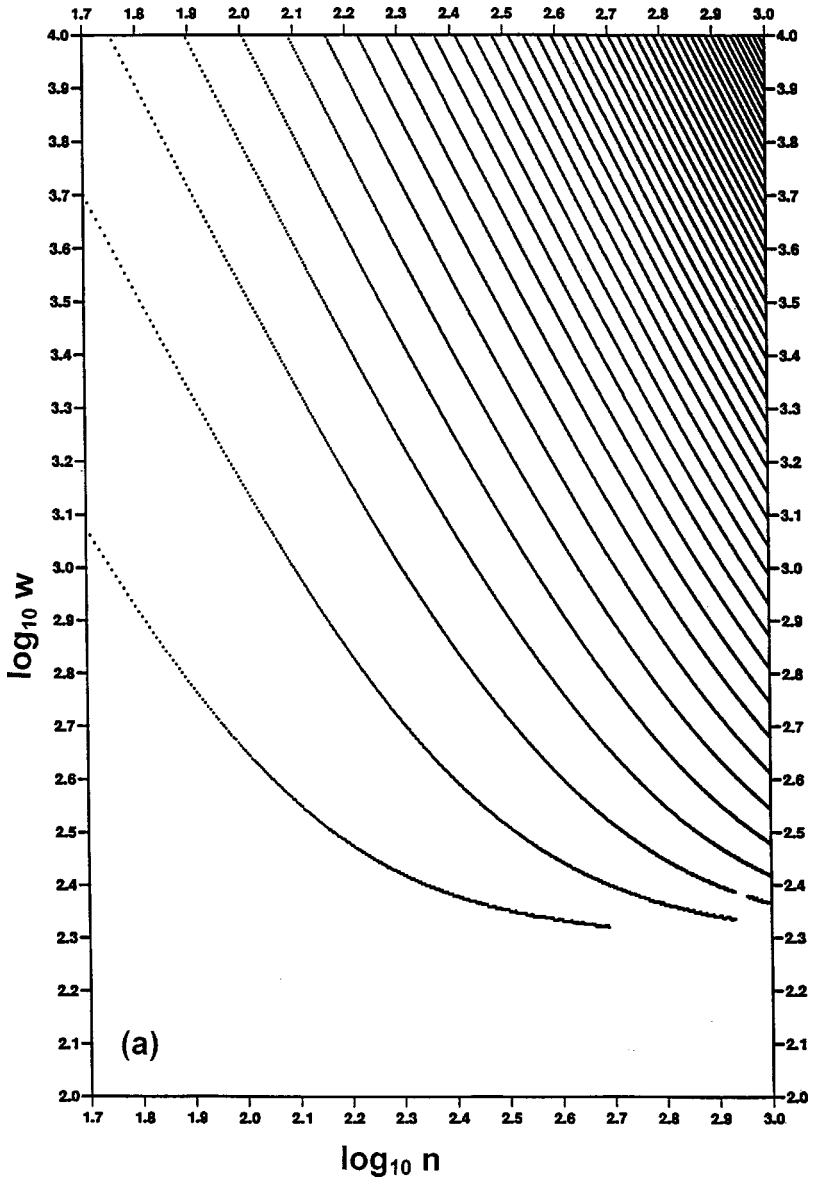

FIG. 9. The effect of exchange parameter on the spin-wave spectrum for a spherical grain with a pinned outer surface and $h=200$ G (a) $J=10^6$ G, (b) $J=5.10^6$ G, and (c) $J=10^7$ G.

an integer number p with the form $c_p \exp(ip\theta)$ for the eigenmagnetization fluctuation. The time-dependent magnetization of resonant modes cannot depend on θ since the resonant field is uniform over the grain size, which is quite smaller than the resonant field wavelength and thus interaction integrals such as

$$\int h_r c_p \exp(ip\theta) d\theta$$

are equal to zero for non-null values of p. Thus in the calculation of transition probabilities, the integration of the angle-dependent magnetization modes all over the grain, leads to the effective interaction of such nonuniform modes with the resonant field to be zero.

Quite similarly, with a granular spherical geometry, as expected here, the equation-of-motion

$$\left[\frac{\partial^2}{\partial r^2}+\frac{2}{r}\frac{\partial}{\partial r}+\frac{1}{r^2\sin^2\varphi}\frac{\partial^2}{\partial\theta^2}+\frac{1}{r^2}\frac{\partial^2}{\partial\varphi^2}+\frac{1}{r^2}\tan\varphi\frac{\partial}{\partial\varphi}+\frac{1}{JM_z}\left(\frac{\omega}{\gamma}-h\right)\right]m=0 \tag{4b}$$

is obtained. Similar arguments of uniformity of the resonant field over the grain, as developed before for cylindrical rods, lead here to consider for resonant modes, only a radial variation of the magnetization, i.e., the only Y_0^0 spherical harmonics. The reason for this is that the spherical averages of the Y_l^m's, which are involved as general solutions of Eq. (4b) are zero if l and m are not simultaneously equal to zero. Similar arguments about effective selection rules in ferromagnetic resonance in grains were given recently by another group.[26] Finally the resulting radial equation of resonant spin motion reads

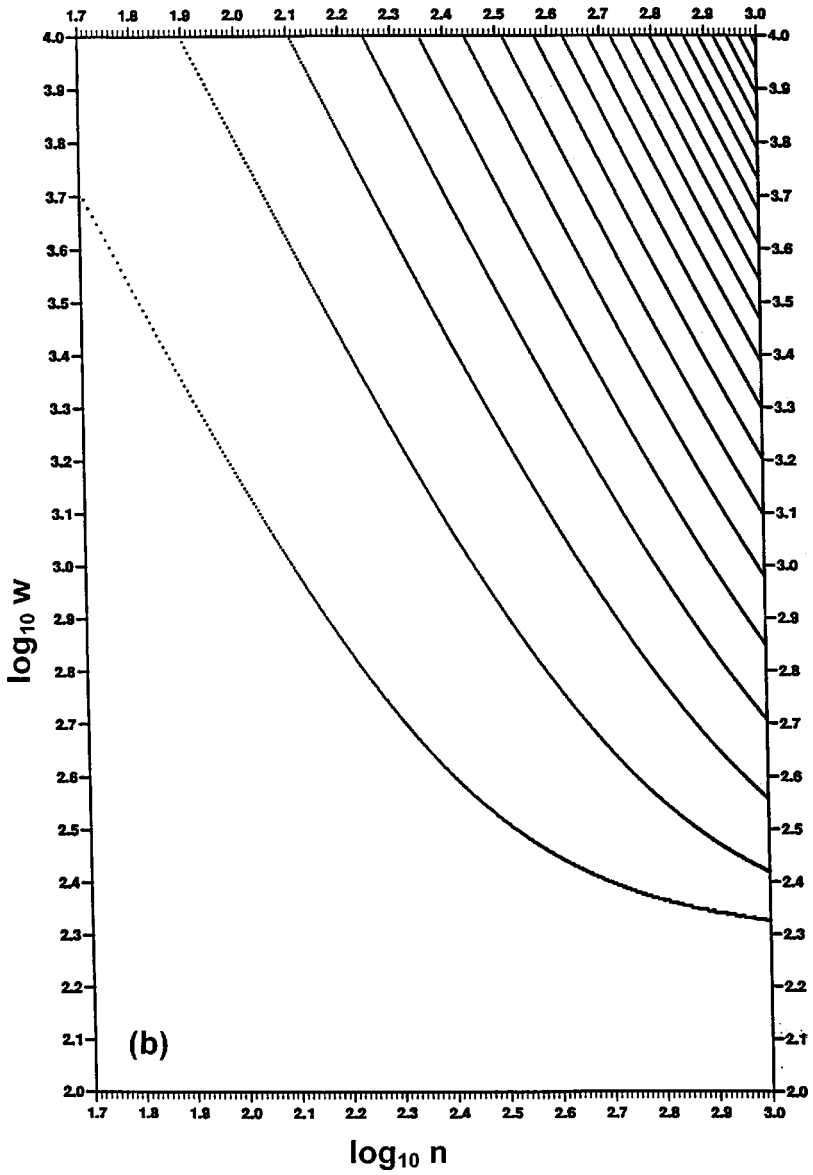

FIG. 9. (*Continued*).

$$\left[\frac{\partial^2}{\partial r^2}+\frac{2}{r}\frac{\partial}{\partial r}+\frac{1}{JM_z}\left(\frac{\omega}{\gamma}-h\right)\right]m=0. \tag{4c}$$

Then with a discrete definition of the spin-wave amplitude b_n at shell n: $b_n=m(r_n)$ and of the radial spin wave derivative on the shell n: $(\nabla b)_r=b_n-b_{n-1}$, this equation-of-motion becomes the discrete equation of resonant spin-wave propagation for the series b_n:

$$b_{n+1}=b_n\left(2+2a-\frac{2}{n}\right)-b_{n-1}\left(1-\frac{2}{n}\right), \tag{5}$$

where the parameter a is a linear function of the eigenfrequency: $a=(1/JM_z)(\frac{\omega}{\gamma}-h)$.

In order to solve this discrete problem of radial wave propagation within a grain, two-by-two transfer matrices with simple definitions of pinning and unpinning on central and outer surfaces, the so called Poincaré's transfer matrices $\mathbf{T}_n$, are introduced.[27] From the mere rewriting of Eq. (5) these matrices are given by

$$\begin{pmatrix} b_{n+1} \\ b_{n+1}-b_n \end{pmatrix}=\mathbf{T}_n\begin{pmatrix} b_n \\ b_n-b_{n-1} \end{pmatrix}, \text{ with}$$

$$\mathbf{T}_n=\begin{pmatrix} 1+2a & 1-\frac{2}{n} \\ 2a & 1-\frac{2}{n} \end{pmatrix}. \tag{6}$$

These ''spherical'' transfer matrices $\mathbf{T}_n$ depend on the shell number n because of spherical grain curvature. This curvature leads the area of successive shells and thus the number of magnetic sites on a shell to increase with the shell radius. It appears for the validity of this approach that the shell number n must be larger than two, with a minimal grain radius of three times the lattice parameter a_0. But this central singularity cannot be observed here where magnetic clusters are large and contain at least thousands of atoms.

Quite similarly ''cylindrical'' transfer matrices $\mathbf{T}'_n$ can be defined for granular rods. In this case a slight difference

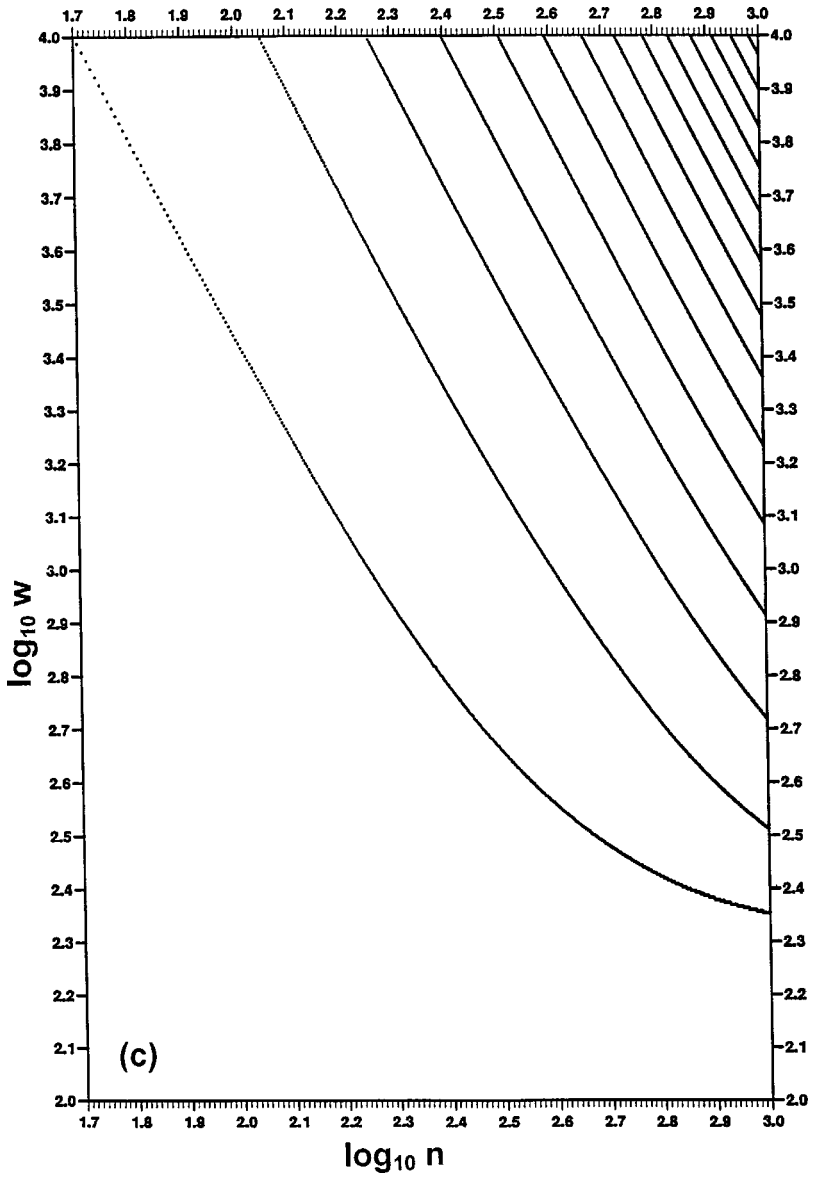

FIG. 9. (*Continued*).

occurs because of the lower increase of the number of neighbors versus radius increase for cylinders than for spheres:

$$\mathbf{T}'_n = \begin{pmatrix} 1+2a & 1-\dfrac{1}{n} \\ 2a & 1-\dfrac{1}{n} \end{pmatrix}. \tag{7}$$

In this case the minimal grain radius would be twice the lattice parameter, which is also a very small size unexpected for realistic grains.

With either cylindrical or spherical grains the boundary conditions for spin waves are no longer symmetric as they usually are for thin films.[27] Here, at the center or at the central axis, continuity of spin waves at the atomic scale implies the occurrence of an unpinned state $b_3 = b_2$. In the continuum model, this continuity argument at the origin leads to select only the regular solution $j_0(kr)$.[12,13,26] At the external surface, the pinning constraint comes from real surface conditions as they occur in thin films.[27] In this paper, the pinning condition at the external surface is assumed to be isotropic. Thus the spin amplitude is a scalar quantity. This assumption corresponds to a simple isotropic surface anisotropy as introduced by Shilov and co-workers.[26] This condition at the outer surface can be any state between perfect pinning where spins at the surface are rigid and perfect unpinning where spins at the surface are free to move. In the general case, the pinning angle ψ at the outer surface is defined by

$$\tan\psi = \frac{b_{N-1}}{b_N}. \tag{8}$$

Finally, the characteristic equation for the spin-wave frequency reads as a scalar product resulting from a matrix product involving the two boundary conditions as well as the radial propagation through the grain:

$$\overbrace{\sin\psi - \cos\psi \quad \cos\psi} \cdot \mathbf{T}_N \cdot \mathbf{T}_{N-1} \cdot \ldots \mathbf{T}_3 \cdot \begin{pmatrix} 1 \\ 0 \end{pmatrix} = 0. \tag{9}$$

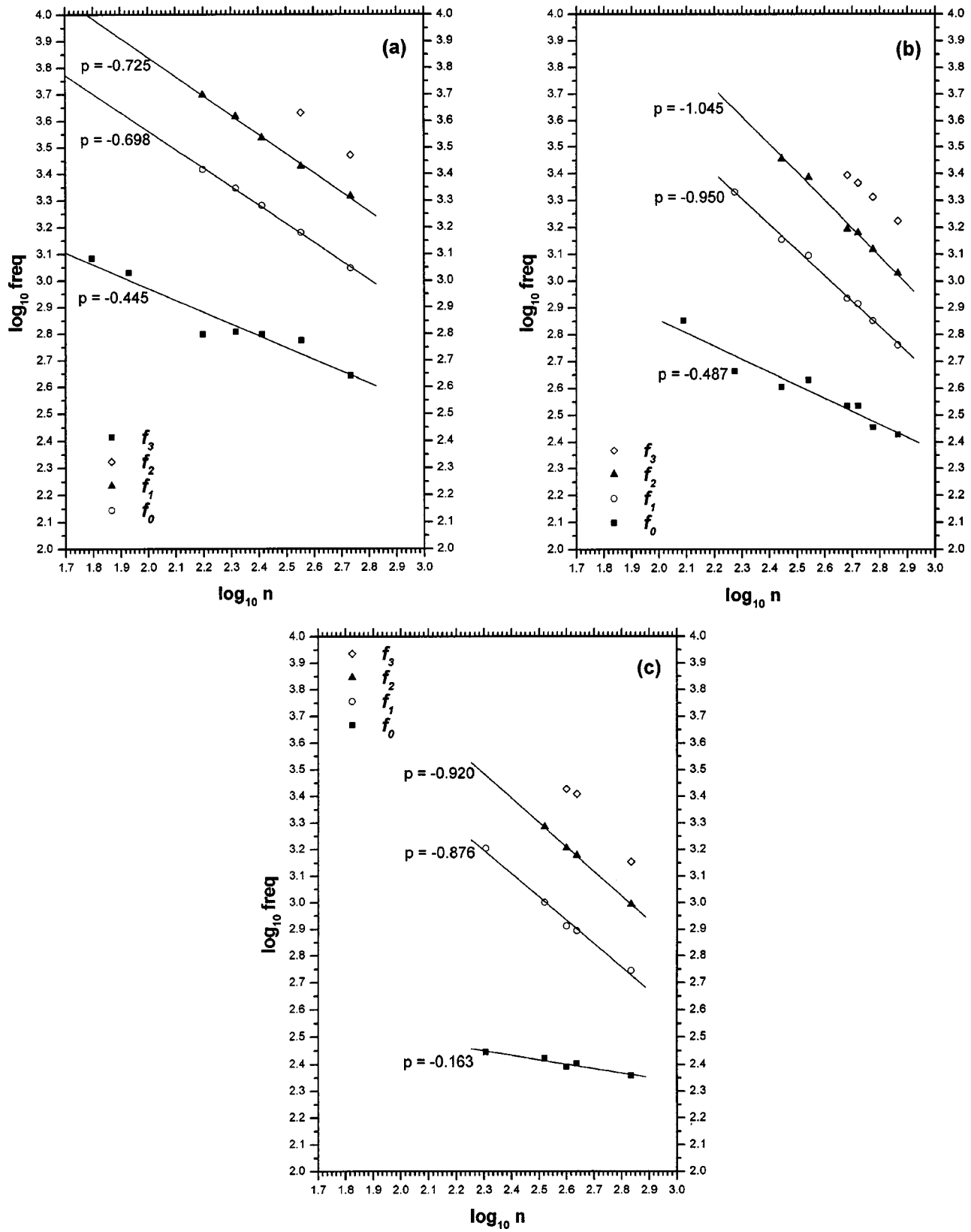

FIG. 10. Resonance frequencies of microwave permeability vs mean radius in a $\log_{10}-\log_{10}$ representation of (a) $Co_{80}Ni_{20}$ particles, (b) $Co_{50}Ni_{50}$ particles, and (c) $Co_{20}Ni_{80}$ particles.

This characteristic equation is a polynomial equation in the parameter a and thus in the rf pulsation ω. It is solved by means of standard numerical methods for different pinning conditions. The corresponding radial spin-wave eigenvectors are then deduced from the successive application of transfer matrices with the eigenpulsation in right order to the central spin and spin gradient vector. The resonant spin-wave profiles in a given rf resonant field are then deduced. The spin-

wave intensities are calculated from the integration of transition probabilities over all sites. That integration favors the first mode where all amplitudes are positive and add, while higher modes with alternate signs are highly compensated and appear with weaker intensities.

A comparison of the numerical result obtained for resonant pulsations in spherical and cylindrical grains with the same magnetic parameters as a function of the grain size is reported in Fig. 7 in a $\log_{10}$-$\log_{10}$ plot, with evidence for a very weak difference between these spectra. Thus the grain shape effect on resonant frequencies is weak. The similar spectra for the same anisotropy field and for both unpinned external surfaces in Figs. 7(a) and 7(b) are characterized by the nearly constant behavior of first modes at large radii, while the higher modes show a nearly R^{-2} law at least for small radii. The lowest resonant frequency is directly determined by the external field h, which is just the anisotropy field. Thus the measurement of the lowest resonant frequency, $\omega = 10^3$ G in Fig. 7(a), enables us to determine the anisotropy field of the sample, here $h = \omega = 10^3$ G. This remark is exact for unpinned outer surfaces and but remains a good approximation for other kinds of outer surface pinning since the resonant frequency of the first modes slowly decreases when the radius increases. Such a behavior with a smooth variation of the lowest mode frequency is shown in Fig. 7(c) in the extreme case of pinned outer surfaces when the other parameters are equal to those of Figs. 7(a) and 7(b). The comparison of Figs. 7(a) and 7(c) shows the part due to partial pinning effects.

The spin-wave profiles of the first three eigenmodes for spherical and cylindrical geometry with the same parameters and radii, are reported in Fig. 8 in the case of pinned outer surfaces for comparison. For a given geometrical shape these profiles are quite different from each other in the number of nodes. Profiles for cylindrical and spherical grains differ and also differ from the wavy modes of a thin film as expected from the different symmetries; they indicate a power-law decrease as continuous Bessel solutions. As a conclusion of the general results reported in Figs. 7 and 8, the eigenfrequencies of resonant spin waves in a grain depend on the grain size in its smaller dimension but depend only weakly on the grain shape. The shape effect is more efficient on the spin-wave profile which is an eigenvector.

The effect of the value of the exchange parameter on the resonance spectra is studied in Fig. 9. Increasing J value has two consequences: first, the gap between the different modes increases; then, the power law of the different modes when the size decreases, including the lowest resonant frequency mode, tends much more rapidly to -2 with the highest J values.

In order to fit the computed resonance spectra with experimental results, two parameters can be varied, the external field h, which is practically close to the local anisotropy field and is defined from the first experimental mode, and the value J of the exchange parameter, which is determined from the frequency difference between the first and second mode for large grains. These parameter values can also be compared to available data for bulk materials with admitted variations due to the change in density between bulk samples and grains.

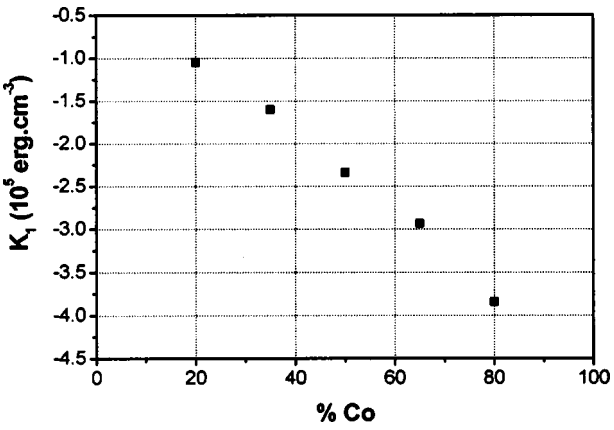

FIG. 11. Anisotropy constant K_1 of $Co_xNi_{(100-x)}$ particles vs cobalt content x inferred from the first resonance frequency ω_0 of large particles (see the text).

Figure 10 shows the size dependence of the experimental resonance frequencies in $\log_{10}-\log_{10}$ representations for several compositions. The experimental number of shells within the particles has been calculated from: $n = R/d$, with R the mean radius and $d = 0.204$ nm the interplanar distance of (111) and (001) dense planes in Co and Ni close-packed phases. As inferred from Fig. 10 the power law is always found lower than 0.5 for the first mode and closer to 1 for the following ones. Such a weak variation of the lowest resonant frequency is in good agreement with the computational results reported in Fig. 7, with evidence for an effective intermediate pinning at the outer surfaces. Thus as shown above, low size dependence of the first mode allows us to estimate the anisotropy field $H_a = \omega_0/\gamma$ from the first resonance frequency ω_0 of large particles, with γ being the gyromagnetic ratio ($\gamma = 2.8$ MHz Oe^{-1}). In case of cubic anisotropy the anisotropy constant K_1 is given by $K_1 = -\frac{3}{4} H_a \times M_s$, with M_s the saturation magnetization of the particle. The K_1 values of $Co_xNi_{(100-x)}$ particles were calculated from the resonance frequency ω_0 for the largest particles ($d = 200$ nm). They present increasing values with increasing cobalt content x (Fig. 11). That result is in good agreement with the expected increase of anisotropy with cobalt concentration of such samples because of the strong crystalline anisotropy of cobalt. Nevertheless, the variation does not exceed one order of magnitude, it is not surprising since the hcp phase is observed only as a minor phase for cobalt-rich composition. A very similar variation was found in previous works for fcc cobalt-nickel bulk alloys[28] and our experimental value for the $Co_{50}Ni_{50}$ composition (-2.35×10^5 erg cm^{-3}) is close to the bulk one which lies between -1.5 and -2.75×10^5 erg cm^{-3}.[28]

Dealing with the frequencies dispersion, the comparison of computational and experimental results in Figs. 9 and 10 shows that in both cases the difference between two successive modes decreases when the order of the modes increases. Nevertheless, an accurate determination of the exchange parameters cannot be obtained. The experimental gap between the successive modes (Fig. 10) is very large and it is the highest value J [Fig. 9(c)] which can describe such a difference between the first and the second mode. Unfortunately

for such high J value the radius exponent is always close to -2 in the computation while its absolute value is found experimentally smaller.

The reason for such a discrepancy is that the assumption of independent grains is probably not valid for higher modes and that magnetic interactions must be taken into account between separate grains in an effective composite material. Another explanation of the low-exponent experimental value could be related to the surface oxidation of the particles and consequently to a nonuniform exchange near the particle surface. This process would lead to a difference between the structural radius and the magnetic radius and to a variation of the pinning condition. Both effects can be easily estimated. These effects are both rather restricted and they cannot explain the observed discrepancy. Thus the main effect for this low power law is the composite effect, that introduces long-ranged contributions because of multiple scattering within the sample. So our conclusion is that the independent grain model is just, to our knowledge, a first approach to this problem.

In the present independent grain model, the spin-wave intensities are easily computed from the spin-wave profiles as explained before. As a matter of fact, the experimental resonance spectra also give evidence for finite linewidths that can be expected to be intrinsic for grains because of the energy dissipation within grains and therefore to weakly depend on the mode nature. So Lorentzian shapes for each resonance line with the same linewidth for all modes are introduced in the computation. The resulting resonance spectrum for a given radius ($n=200$, $R=40$ nm) is reported in Fig. 12 with a realistic value of the linewidth $\Delta h=500$ G and an anisotropy of $h=3000$ G in order to compare with the experimental results of Fig. 4. The lines on the frequency axis give the resonant frequencies that are weighted by the intensities and the shape function. This spectrum (Fig. 12) agrees qualitatively with the experimental one for the same particle mean diameter [Fig. 4(b)]. In both cases the lowest-frequency mode is the first one in intensity scale. As seen experimentally in Figs. 3 and 4(a), for largest particles, the first mode is no more the first one in intensity. That results from an approximate balance between the general weakening of higher modes and their practical overlapping in frequency. This observed feature is linked to the abundance of higher modes that are rather close in energy even if they are individually weak in intensity.

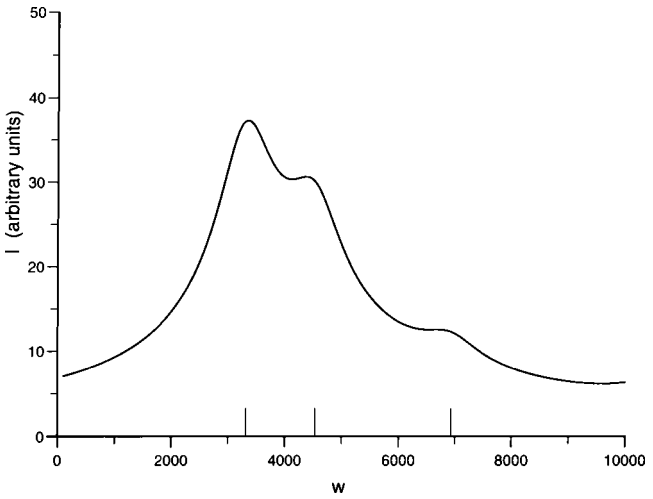

FIG. 12. The effect of linewidth $\Delta h=500$ G and anisotropy $h=3000$ G on the intensity spectrum of spherical grains with $J=5.10^6$ G and $n=200$.

V. CONCLUSION

Spherical and monodisperse magnetic metal particles of various compositions with sizes varying from submicrometer to nanometer size range, were produced by a chemical process in a reproducible way. Their resonance spectra were studied in the absence of an external field in the 0.1–18 GHz range; they present several resonance bands related to nonuniform resonance modes. The large size and composition ranges available by the synthesis process provided an extended set of resonant spectra that allows us to follow accurately the dependence of the resonance frequencies with particle size and composition and to compare with theoretical results. The resonance frequencies are shifted toward high frequencies either when the particle size decreases or when the cobalt content increases in the particle composition. A theoretical model based on a discrete treatment of the resonant effect in independent grains has been developed. This model allows us to compute easily the resonance frequencies, the spin-wave profiles, and their intensity. It allows us, as well, to study the respective influence of the particle geometry, surface pinning, crystalline anisotropy, and exchange parameter values. The role of these different parameters on the size dependence of the resonant modes has been stressed. The analysis of the experimental spectra on the basis of this model enabled us to show that the weak size dependence of the lowest-frequency mode is due to a weak pinning condition at the particle surface. It allowed us to correlate this resonant mode with the magnetic crystalline anisotropy of the samples. Thus, the low-frequency part of the particle permeability is well understood through this model while the high-frequency part involves multiple scattering within the set of grains and thus requires a more sophisticated approach. These interactions made of the grain set a real complex composite material.

*Author to whom correspondence should be addressed. FAX: +(33) 1 46 33 94 01. Electronic address: levy@ccr.jussieu.fr

[1] S. Sugano, *Microcluster Physics*, Springer Series in Material Sciences (Springer, Berlin, 1991); *Clusters of Atoms and Molecules*, edited by H. Haberland, Springer Series in Chemical Physics (Springer, Berlin, 1994), Vols. 52 and 56.

[2] J. R. Childress and C. L. Chien, Phys. Rev. B **43**, 8089 (1991).

[3] S. Gangopadhyay, G. C. Hadjipanayis, B. Dale, C. M. Sorensen, K. J. Klabunde, V. Papaefthymiou, and A. Kostikas, Phys. Rev. B **45**, 9778 (1992).

[4] M. Respaud, J. M. Broto, H. Rakoto, A. R. Fert, L. Thomas, B. Barbara, M. Verelst, E. Snoeck, P. Lecante, A. Mosset, J. Osuna, T. Ould Ely, C. Amiens, and B. Chaudret, Phys. Rev. B **57**, 2925 (1998).

[5] F. Fiévet, J. P. Lagier, and M. Figlarz, in *Powder Metallurgy 94* (Les Editions de Physique, Les Ulis, France, 1994), Vol. 1, p.

281.
[6] J. P. Chen, C. M. Sorensen, K. J. Klabunde, and G. C. Hadji panayis, J. Appl. Phys. **76**, 6316 (1994).
[7] C. Petit, A. Taleb, and M. P. Pileni, J. Phys. Chem. **103**, 1805 (1999).
[8] J. A. Blackman, B. L. Evans, and A. I. Maaroof, Phys. Rev. B **49**, 13 863 (1994).
[9] A. Berkowitz, J. R. Mitchell, M. J. Carey, A. P. Young, S. Zhang, F. E. Spada, F. T. Parker, A. Hutton, and G. Thomas, Phys. Rev. Lett. **68**, 3745 (1992).
[10] J. Barnas and A. Fert, Phys. Rev. Lett. **80**, 1058 (1998).
[11] C. Kittel, Phys. Rev. **110**, 1295 (1958).
[12] A. Aharoni, J. Appl. Phys. **69**, 7762 (1991).
[13] A. Aharoni, J. Appl. Phys. **81**, 830 (1997).
[14] P. A. Voltairas and C. V. Massalas, J. Magn. Magn. Mater. **124**, 20 (1993).
[15] G. Viau, F. Fiévet-Vincent, F. Fiévet, P. Toneguzzo, F. Ravel, and O. Acher, J. Appl. Phys. **81**, 2749 (1997).
[16] G. Viau, F. Fiévet-Vincent, and F. Fiévet, Solid State Ionics **84**, 259 (1996).
[17] G. Viau, F. Fiévet-Vincent, and F. Fiévet, J. Mater. Chem. **6**, 1047 (1996).
[18] Ph. Toneguzzo, G. Viau, O. Acher, F. Fiévet-Vincent, and F. Fiévet, Adv. Mater. **10**, 1032 (1998).
[19] Ph. Toneguzzo, G. Viau, O. Acher, F. Guillet, E. Bruneton, F. Fiévet-Vincent, and F. Fiévet, J. Mater Sci. (to be published).
[20] G. K. Williamson and W. H. Hall, Acta Metall. **1**, 22 (1953).
[21] Ph. Toneguzzo, Ph.D. thesis, Université Paris 7, Denis Diderot, 1997; P. Toneguzzo, O. Archer, G. Viau, A. Pierrard, F. Fiévet-Vincent, and I. Rosenman, IEEE Trans. Magn. **35**, 3469 (1999).
[22] A. Berthault, D. Rousselle, and G. Zerah, J. Magn. Magn. Mater. **112**, 477 (1992); D. Rousselle, A. Berthault, O. Acher, J. P. Bouchaud, and G. Zerah, J. Appl. Phys. **74**, 475 (1993).
[23] G. Viau, F. Ravel, O. Acher, F. Fiévet-Vincent, and F. Fiévet, J. Magn. Magn. Mater. **140-144**, 377 (1995); L. Olmedo, G. Chateau, C. Deleuze, and J. L. Forveille, J. Appl. Phys. **73**, 6992 (1993).
[24] D. Wei and G. N. Patey, Phys. Rev. Lett. **68**, 2043 (1992).
[25] J. J. Weis and D. Lévesque, Phys. Rev. Lett. **71**, 2729 (1993).
[26] V. P. Shilov, J.-C. Bacri, F. Gazeau, F. Gendron, R. Perzynski, and Y. L. Raikher, J. Appl. Phys. **85**, 6642 (1999).
[27] D. Mercier, J.-C. S. Lévy, M. L. Watson, J. S. S. Whiting, and A. Chambers, Phys. Rev. B **43**, 1433 (1991); J.-C. S. Lévy, Surf. Sci. Rep. **1**, 39 (1981); H. Puszkarski, *ibid.* **20**, 191 (1994).
[28] Landolt-Börnstein, *Magnetic Properties, New Series III/19a* (Springer, Berlin, 1982), p. 219.